IEEE Access
Multidisciplinary ⋮ Rapid Review ⋮ Open Access Journal

Received January 12, 2022, accepted January 24, 2022, date of publication February 2, 2022, date of current version February 14, 2022.

Digital Object Identifier 10.1109/ACCESS.2022.3148740

Co-Circularly Polarized Planar Antenna With Highly Decoupled Ports for S-Band Full Duplex Applications

HAQ NAWAZ[1], AHMAD UMAR NIAZI[2], AHSEN TAHIR[1], NOMAN AHMAD[3], USMAN MASUD[2], TURKE ALTHOBAITI[4,5], ABDULLAH ALHUMAIDI ALOTAIBI[6], AND NAEEM RAMZAN[7], (Senior Member, IEEE)

[1]Department of Electrical Engineering, University of Engineering and Technology, Lahore 54890, Pakistan
[2]Department of Electronics Engineering, University of Engineering and Technology (UET) Taxila, Taxila 47050, Pakistan
[3]Research Institute for Microwave and Millimeter-Wave Studies (RIMMS), National University of Sciences and Technology (NUST), Islamabad 44000, Pakistan
[4]Department of Computer Science, Faculty of Science, Northern Border University, Arar 73222, Saudi Arabia
[5]Remote Sensing Unit, Northern Border University, Arar 73222, Saudi Arabia
[6]Department of Science and Technology, College of Ranyah, Taif University, Taif 21944, Saudi Arabia
[7]School of Computing, Engineering and Physical Sciences, University of the West of Scotland, Paisely PA1 2BE, U.K.

Corresponding author: Haq Nawaz (haq.nawaz@uet.edu.pk)

This work was supported in part by the Deputyship for Research and Innovation, Ministry of Education, Saudi Arabia, under Project IF_2020_NBU_004; and in part by the Taif University, Taif, Saudi Arabia, through the Taif University Research Grant under Project TURSP-2020/277.

ABSTRACT This work presents a unidirectional, co-circularly polarized (CP), printed antenna with highly decoupled or isolated transmit (T_x) and receive (R_x) ports for 2.4 GHz in-band full duplex (IBFD) applications. The presented antenna topology is based on four similar and sequentially rotated trimmed patches with right hand circular polarized (RHCP) characteristics. The symmetrical placement of two T_x patches with respect to both R_x elements results in equal levels of self interference (SI) which was suppressed through balanced excitation of T_x mode. This mechanism results in effective suppression of SI at each R_x patch. The residual SI is suppressed further through a second balanced feeding network deployed at $R_x$port of proposed antenna topology. The employed balanced feeding networks provide superior performance of $\leq$ 0.5 dB and 6° magnitude and phase imbalances respectively between the two balanced output ports over the bandwidth of interest. The measured results for prototype of presented antenna achieve -10 dB bandwidth of better than 100 MHz for both T_x and $R_x$ports. The measured interport coupling for validation model $\leq$ -70 dB across the entire bandwidth of 100 MHz. As per best of authors' knowledge, the presented antenna is the first one to report such reduced levels of interport coupling over the whole impedance bandwidth of planar antenna with unidirectional radiation patterns and co-RHCP characteristics for both T_x and R_x modes across the overlapped bandwidth.

INDEX TERMS Circularly polarized antenna, unidirectional radiation pattern, reduced interport coupling, self interference suppression, balanced feeding network.

I. INTRODUCTION

The future communication systems require novel and efficient duplexing techniques to offer higher data rates through improved spectral efficiency for wireless links [1], [2]. Such duplexing schemes should utilize the available bandwidth effectively to achieve higher throughputs [1], [2]. The in-band full duplex (IBFD) scheme also known as single frequency full duplex (SFFD) can theoretically double the spectral efficiency or link capacity through concurrent transmission and reception over the same bandwidth [3]–[6]. However, such simultaneous transmission and reception operation across the overlapping bandwidth results in strong co-channel coupling or self interference (SI) between the transmit (T_x) node and co-located receive (R_x) node. Due to such strong in-band coupling, the SI power levels are much higher than those of the desired signal levels [3], [4]. Such strong co-channel interference degrades the capacity of R_x channel through reduced signal to interference ratio for IBFD links [6]. In fact, the strong in-band SI signals act as jamming signals to

The associate editor coordinating the review of this manuscript and approving it for publication was Hassan Tariq Chattha.

overpower the desired R_x signals [7]. The resulting in-band coupling or SI is comprised of both direct T_x power leakage to R_x channel and coupling of reflected T_x signals (from surrounding objects) to its own R_x node [8]. Furthermore, the former type of complex SI is comprised of both linear and non-linear components of T_x signals [8].

The successful realization of IBFD operation requires the effective suppression or mitigation of SI at R_x node to provide the intended inter-node isolation levels [7], [8]. Due to presence of very strong T_x signals, significant levels of self interference cancellation (SIC) is required on R_x node to provide the intended isolation levels for effective retrieval of low powered R_x signals [7], [8]. The ideal case will be the suppression of SI signals to the inherent noise floor of receiver so that the desired signals from remote transmitter can be detected successfully [7], [8]. Practically, the intended SIC levels are defined by the T_x power, noise figure and desired bandwidth of the IBFD transceiver [7]. The required high levels of T_x-R_x isolation demand the SIC operation at multiple stages (including frontend of transceiver and digital base band stage) across the IBFD transceiver [8]–[10]. Moreover, it is essential to achieve higher SIC levels at transceiver's front end (antenna stage and RF domain) comparative to other SI suppression stages in order to preserve the dynamic range of ADC for desired R_x signals [11], [12]. This will also alleviate the required isolation levels imposed on later SIC stages of transceiver.

So far, various SIC techniques have been investigated to clinch elevated levels of interport isolation for antennas intended for IBFD applications [13]–[25]. The SIC techniques include the path loss decoupling based on spatial separation of antennas elements [13], isolation through uncorrelated dual polarized $T_x$and R_x signals [14]–[19], suppression of SI through near field cancellation i.e. near field SIC [20]–[22], and other topologies based on characteristics modes and different polarizations for $T_x$and R_x modes [23]–[25]. The path loss based isolation termed as spatial duplexing acquires the decoupling between $T_x$and $R_x$ports of IBFD antennaby increased spacing between T_x and R_x antenna elements or through separation of very narrow directional beams from respective antennas.

The dual polarization based isolation techniques exploit the intrinsic decoupling of orthogonal T_x and R_x signals to achieve up to 40 dB and 20 dB port to port isolation for linearly-polarized [18]–[20] and circularly-polarized antennas [15]–[17] respectively. Moreover, the dual polarized stacked printed antennas based on hybrid feeding networks can offer around 20 dB additional levels of isolation on the top of polarization isolation [26]. The interport isolation levels for such dual polarized antennas can be improved further through analog or RF domain SIC stages based on signal inversion techniques [26]–[28]. However, the achievable SIC bandwidth through such techniques is limited to few MHz and can be improved on the cost of additional complexity and power loss [27]. Furthermore, the polarization based decoupling techniques restrict the IBFD transceivers to employ the polarization duplexing for bidirectional communication where the forward and reverse links use different polarizations. Moreover, the polarization based duplexing is not viable in wireless systems intended for several applications including the continuous-wave radar systems based on shared or single antenna architectures [29]–[31]. In addition, the bidirectional wireless systems employing the same polarization for forward and reverse channels to safeguard the channel reciprocity to facilitate the second polarization for an additional full duplex link [32]. For instance, the linear vertical polarization can be used for first bidirectional link while the second full duplex link can utilize the linear horizontal polarization [33]. The intrinsic isolation of polarization duplexing will provide sufficient levels of isolation between two bidirectional links in that case. However, the polarization mismatch loss may still arise due to misalignment of co-polarized antenna employed at respective T_x and R_x nodes. The resulting polarization mismatch loss can be avoided effectively through the co-circularly polarized (same CP polarization) antennas. In that case, the left handed circular polarization (LHCP) or right hand circular polarization (RHCP) can be used for each full duplex wireless link. However, the dual port, compact co-polarized CP antennas with significant levels of interport isolation are essential for such links.

Recently, the interport isolation techniques based on near field SIC topologies have been emerged to achieve excellent isolation levels through compact printed antennas [33]–[37]. Such techniques are equally effective for single antenna element [33]–[36] and antenna array configurations [37]. Moreover, these techniques provide nice SIC performance both for shared antenna and separate antenna architectures. Furthermore, the near field SIC techniques are well efficient both for dual polarized and co-polarized antennas to achieve either directional or omnidirectional radiations. However, the achievable isolation performance of near field SIC techniques rely on the characteristics of the employed feeding networks and symmetry of R_x elements/ports with respect to T_x element/port [33]–[37].

This work presents an antenna array configuration based on four trimmed patches to achieve right handed circular polarization and unidirectional radiation patterns for both T_x and R_x modes. The well-balanced feeding networks for each pair of T_x and R_x antenna elements achieve very high levels of port to port isolation through near field SIC operation. The employed balanced feeding networks achieve the high interport isolation without degradation in radiation features of presented co-circularly polarized antenna array. The structure of each feeding network is comprised of two inverted microstrip arms as output balanced ports and input unbalanced port excited through H-shaped slot in ground plane. The proposed IBFD antenna array and feeding networks have been implemented and interconnected to record the measurement results.

The rest of this paper is organized in following way: The section II presents the topology of proposed antenna array

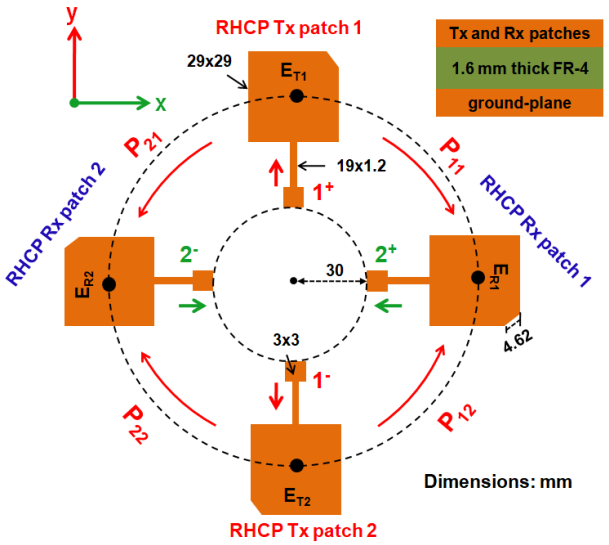

FIGURE 1. The architecture of proposed co-RHCP antenna comprised of four identical and sequentially rotated RHCP patches.

based on two pairs of $T_x$and R_x patches. The passive SIC operation for the case of ideal balanced feeding is described mathematically in this section too. This section also provides the full-wave simulation results for the proposed IBFD antenna with co-RHCP characteristics. The implementation details for the validation model of proposed antenna array are presented in section III. The novelty and contributions of this work are detailed in section IV. Followed by, the conclusions in section V.

II. ARCHITECTURE OF PROPOSED Co-CP ANTENNA ARRAY WITH PASSIVE SIC MECHANISM

The geometry of the proposed co-RHCP antenna array and its dimensions are presented in Fig. 1 for the operating frequency of 2.4 GHz. The architecture of presented antenna is based on four identical and sequentially rotated patches with RHCP characteristics. As depicted in Fig. 1, the four sequentially rotated antenna elements or patches have been placed symmetrically with respect to each other. Each patch is corner-trimmed to generate RHCP through single feed or port. As indicated in Fig. 1, two diametrically opposite pairs of RHCP patches have been used for differentially excited (balanced-fed) T_x and R_x. The balanced feeding operation will be realized through a compact and wideband slot-coupled balanced feeding network. As indicated in Fig. 1, a single layered FR-4 substrate with 1.6 mm thickness, relative permittivity (ε_r) of 4.4 and loss-tangent ($\tan\delta$) $=$ 0.02; has been used for design and implementation of presented co-CP antenna array.

The trimmed-corner, square-shaped T_{x1} patch radiates a RHCP wave when excited from port 1^+ through a thin coplanar feed line. The radiated RHCP wave is comprised of two orthogonal and equi-magnitude components of E fields. The phasor form representation of E fields from both pairs of

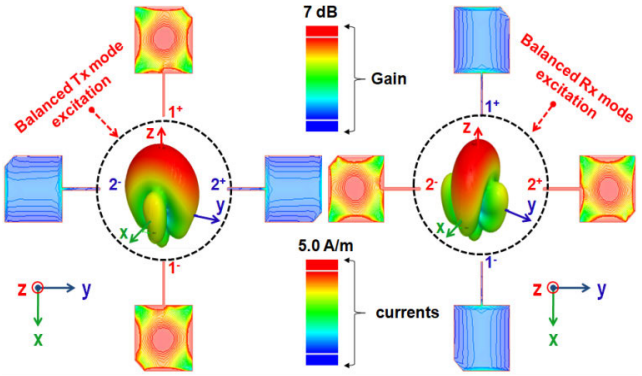

FIGURE 2. The HFSS simulated surface current intensities and 3D gain patterns at f = 2.45 GHz for balanced T_x and R_x excitations through respective ports of proposed co-RHCP antenna.

T_x and R_x patches can be expressed as follows:

$$\boldsymbol{E}_{T1} = \boldsymbol{E_o}\left(\hat{x} - j\hat{y}\right), \quad \boldsymbol{E}_{T2} = e^{-j180^o}\boldsymbol{E_o}\left(\hat{x} - j\hat{y}\right) \tag{1}$$

$$\boldsymbol{E}_{R1} = e^{-j90^o}\boldsymbol{E_o}\left(\hat{x} - j\hat{y}\right), \quad \boldsymbol{E}_{R2} = e^{-j270^o}\boldsymbol{E_o}\left(\hat{x} - j\hat{y}\right) \tag{2}$$

where $\hat{x}$ and $\hat{y}$ represent the unit vectors along x and y dimensions respectively and $\boldsymbol{E_o}$ denotes the peak amplitude of radiated electric field ($\boldsymbol{E}$).

For balanced-fed or differentially excited pair of T_x ports (1^+ and 1^-) of antenna presented in Fig. 1, the resultant electric field vector ($\boldsymbol{E_T}$) can be computed as:

$$\boldsymbol{E}_T = \boldsymbol{E_{T1}} + e^{j180^o}\boldsymbol{E_{T2}}$$
$$\boldsymbol{E}_T = 2 * \left[\boldsymbol{E_o}\left(\hat{x} - j\hat{y}\right)\right] = \mathbf{2} * \boldsymbol{E}_{T1} \tag{3}$$

Similarly, the resulting electric field vector ($\boldsymbol{E_R}$) for differentially excited R_x mode through pair of R_x ports (2^+ and 2^-) of proposed antenna array is given as:

$$\boldsymbol{E}_R = \boldsymbol{E_{R1}} + e^{j180^o}\boldsymbol{E_{R2}}$$
$$\boldsymbol{E}_R = 2 * \left[e^{-j90^o}\boldsymbol{E_o}\left(\hat{x} - j\hat{y}\right)\right] = \mathbf{2} * \boldsymbol{E}_{R1} \tag{4}$$

As evident from (3), the balanced or differential feeding through pair of T_x ports of proposed antenna results in constructive combination (in-phase addition) of electric fields generated from each T_x patch. Similar is the case for the incident (received) electric fields through the differential output operation for pair of R_x ports of antenna presented in Fig. 1 as clear from (4). Furthermore, the radiated (transmitted) and incident (received) signals from each pair of balanced-fed or differentially excited T_x and R_x patches are right hand circular polarized (RHCP) as evident from the resulting E fields expressed by (3) and (4). The co-RHCP characteristics of presented antenna are also validated by the full-wave simulations through Ansoft HFSS software. The simulated surface currents densities and three dimensional radiation patterns for differentially excited T_x and R_x modes are exhibited in Fig. 2 to endorse the in-phase addition of E fields for each pair of patches.

The presented antenna architecture provides very low levels of coupling (high isolation) between the single-ended T_x and R_x ports due to effective cancellation of SI at designated $R_x$port. The reduced interport coupling mechanism based on balanced feeding at T_x and R_x ports can be investigated through a very simple analysis. As evident from the geometry of proposed antenna in Fig. 1, the symmetrical placement of both R_x elements with respect to T_x elements generates same levels of SI (in-band coupling from T_x to R_x patches). Moreover, the two components of SI at each R_x patch have phase difference of 180° degree due to the differential excitation of T_x patches. Assume that P_{11}, P_{12} P_{21} and P_{22} denote the SI levels (in dB) for each pair of T_x-R_x patches. The SI power (P_{SI}) at port 2^+ and $2^-$of both R^x patches can be expressed as follows:

$$\boldsymbol{P}_{\mathrm{SI}}{}^{2+} = \boldsymbol{P}_{11} - \boldsymbol{P}_{12} \quad \text{and} \quad \boldsymbol{P}_{\mathrm{SI}}{}^{2-} = \boldsymbol{P}_{21} - \boldsymbol{P}_{22} \tag{5}$$

Based on the symmetry of the presented antenna structure $\boldsymbol{P}_{11} = \boldsymbol{P}_{12} = \boldsymbol{P}_{21} = \boldsymbol{P}_{22}$ and SI should be completely suppressed (infinite isolation) at the output of each R_x patch in ideal case. However, in practice $\boldsymbol{P}_{11} \cong \boldsymbol{P}_{12} \cong \boldsymbol{P}_{21} \cong \boldsymbol{P}_{22}$ to offer finite levels of isolation between each pair of T_x-R_x patches and achieved isolation levels are dependent on balancing characteristics of employed feeding network for differential excitation of T_x mode. Furthermore, the isolation levels can be improved by suppressing the residual SI ($\boldsymbol{P}_{\mathrm{SI}}{}^{2+}$ and $\boldsymbol{P}_{\mathrm{SI}}{}^{2-}$) through differential R_x operation. This mechanism will improve the isolation levels through following SIC operation where the SI power ($\boldsymbol{P}_{\mathrm{SI}}$) at single-ended or unbalanced port of differential circuit can be expressed through following relation:

$$\boldsymbol{P}_{\mathrm{SI}} = \boldsymbol{P}_{\mathrm{SI}}{}^{2+} - \boldsymbol{P}_{\mathrm{SI}}{}^{2-} \tag{6}$$

As $\boldsymbol{P}_{\mathrm{SI}}{}^{2+}$ and $\boldsymbol{P}_{\mathrm{SI}}{}^{2-}$ powers are already very low so the second stage of suppression will provide very high levels of isolation between single ended or unbalanced ports T_x and R_x ports of presented co-RHCP antenna structure.

It is evident from above analysis that the differential excitation for each pair of T_x and R_x patches can offer very high interport isolation levels without compromising the radiation performance of the proposed antenna. However, the achievable isolation levels for the presented antenna structure are highly dependent on the in-band amplitude and anti-phase balancing characteristics of the differential feeding networks. Moreover, the well-balanced T_x and R_x modes can also provide the improved gain performance for presented antenna through low side lobe levels (SLL).

For instance, the ideal balanced feeding networks can achieve ≥80 dB isolation across the entire −10 dB bandwidths of $T_x$and R_x ports as clear from the simulation results presented in Fig. 3. As evident from these simulation results, the −10 dB bandwidth for both T_x and R_x ports is better than 100 MHz and free space path loss based isolation between each pair of T_x-R_x patches is around 27 dB across the 100 MHz bandwidth. Based on (5), an ideal differentially

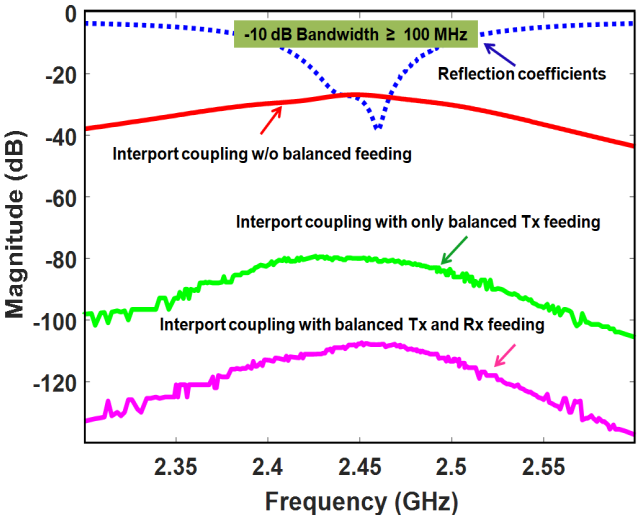

FIGURE 3. The simulated reflection-coefficients and interport coupling levels for presented antenna with balanced T_x and R_x feeding.

excited T_x mode improves the isolation levels to ≥80 dB across the bandwidth of interest. The interport isolation levels of better than 100 dB are achieved through an ideal differential-fed R_x mode which cancels the residual SI as evident from (6). However, the resulting isolation levels through practical balanced feeding networks will be degraded due to non-ideal response of such networks.

It is evident from above discussions that the performance (amplitude and phase balances) of the balanced feeding network defines the achievable SIC levels for presented antenna structure. In this work, a modified version of a differential circuit (balun) reported in [38] has been used for balanced excitation of presented antenna. Two such symmetrical baluns have been used for balanced excitation of T_x and R_x modes. The geometry of modified wideband balun and its dimension are given in Fig. 4. The presented balun realizes the desired differential characteristics through a pair of microstrip to slot-line transitions. The narrow H-shaped slot-line in the ground plane provides the required coupling between the unbalanced port and the pair of balanced ports. The presented balun circuit is designed and implemented on a 1.6 mm thick FR-4 substrate with permittivity (ε_r) of 4.4 and loss-tangent ($\tan\delta$) = 0.02.

The geometrical dimensions of microstrip to slot-line transition based balun (balanced network) are detailed in Fig. 4. The simulation results like reflection coefficients, magnitude and the phase balance characteristics of proposed balun are detailed in Fig. 5. The port 1 is the unbalanced port while port 2 and port 3 are balanced ports of proposed balun. As clear from these simulated characteristics, the presented balun or balanced feeding network exhibits very low levels of reflections (well matched ports) for unbalanced and pair of balanced ports and -10 dB bandwidths are in excess of 1 GHz. As clear from Fig. 5, the simulated amplitude and phase errors are ≤0.09 dB and ≤0.15° respectively across the bandwidth of interest (100 MHz) spanning over 2.40 GHz

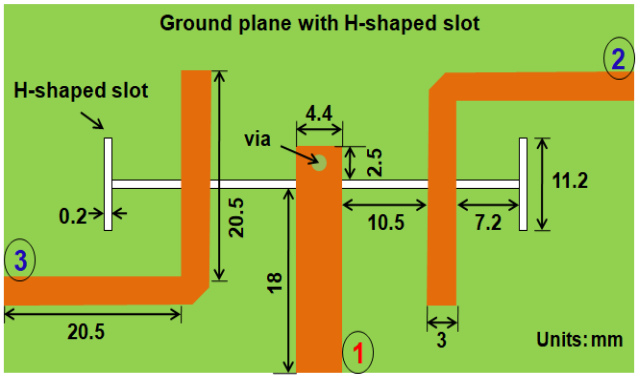

FIGURE 4. EM Model and geometrical dimensions of the proposed microstrip to slot-line transition based balun (balanced network).

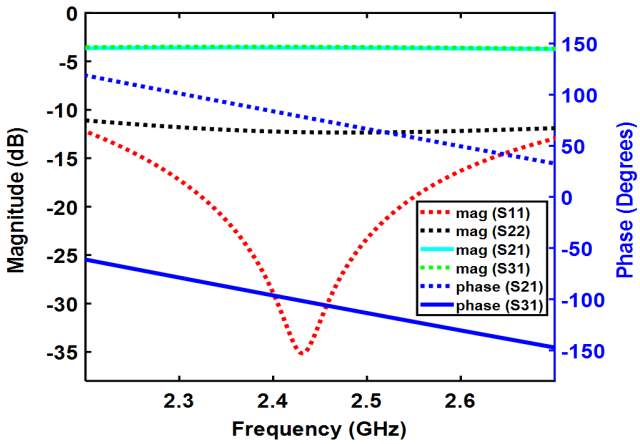

(a)

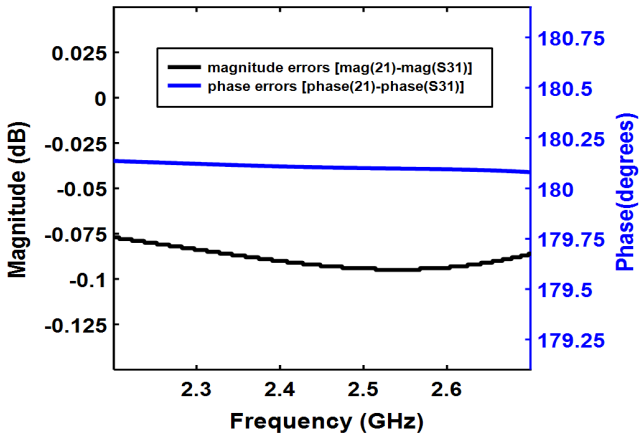

(b)

FIGURE 5. The simulated results for presented microstrip to slot-line transition based balun (a) reflection coefficients, magnitude and phase responses (b) magnitude and phase imbalances (errors).

to 2.50 GHz. The insertion loss of the presented balun is less than 0.5 dB across the intended bandwidth as clear from Fig. 5(a). These improved characteristics of balun offer the potential of achieving high SIC levels through balanced T_x and R_x excitations of presented co-RHCP antenna.

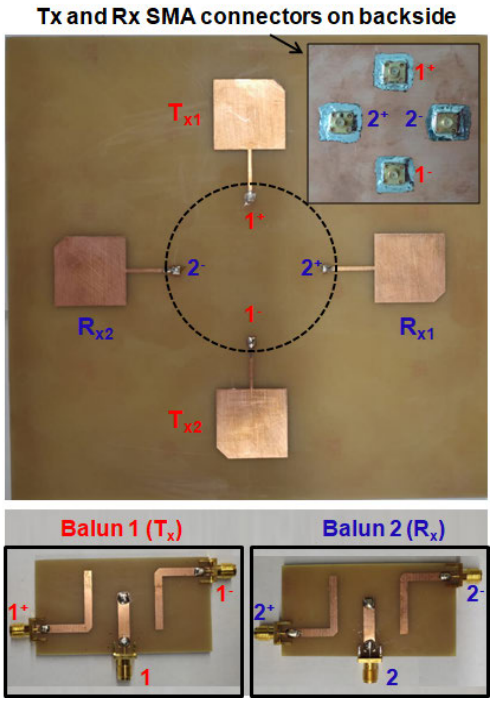

FIGURE 6. The validation models of antenna and two slot-fed baluns for balanced T_x and R_x feeding of two pairs of co-RHCP patches.

III. EXPERIMENTAL CHARACTERISTICS OF PRESENTED Co-RHCP ANTENNA SYSTEM

In order to ensure the T_x, R_x ports matching, interport isolation (decoupling) performance and validate the far-field characteristics of the presented antenna system, a prototype (validation model) of antenna system was implemented using basic printed circuit board (PCB) technology. The antenna array and two baluns were implemented on FR-4 substrate having $\varepsilon_r = 4.4$, $\tan\delta = .02$ and thickness of 1.6mm. The validation models of antenna-elements and both of the baluns is shown in Fig. 6. The sub-miniature (SMA) connectors have been mounted / soldered on designated ports of antenna-elements (on back side of patches) and both baluns. The T_x and R_x baluns will be connected to respective ports of antenna-elements through phase-matched cables as indicated in Fig. 7(a).

The validation model was characterized through measurements with a calibrated vector network analyzer (VNA) shown in Fig. 7(a) to record its T_x and R_x ports matching and interport isolation parameters The simulated and measured S-parameters for presented antenna system are depicted in Fig. 7(b). Note that the simulated S-parameters for the antenna system were obtained through the interconnections of EM models of antenna-elements and baluns in schematic. This implies that the effects of phase-matched cables and SMA connectors were not considered in simulations. As indicated in Fig. 7(b), the presented antenna system offers −10 dB bandwidth in excess of 100 MHz which spans over 2.40 GHz to 2.50 GHz for both T_x and R_x ports. In addition, the assembled antenna system offers better than

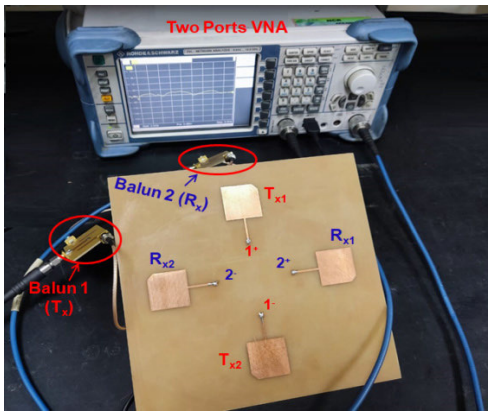

(a)

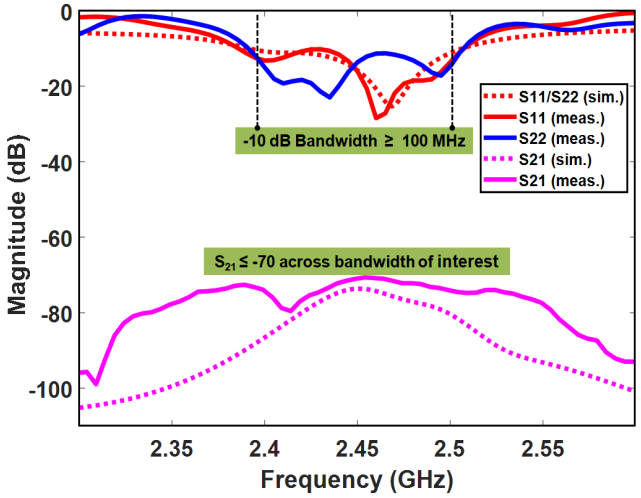

(b)

FIGURE 7. (a) Test and measurement setup for S-parameters characterization (b) The simulated and measured port matching and interport coupling results for the validation model of antenna.

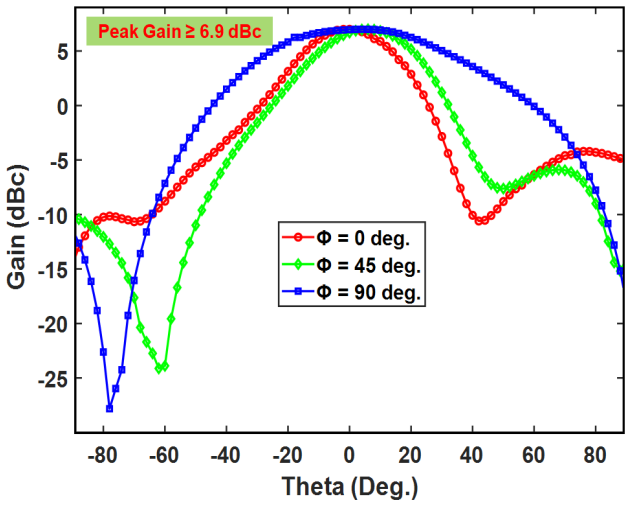

FIGURE 8. The measured gain levels for T_x mode at operational frequency of 2.45 GHz with $\Phi = 0°$, 45° and 90° cuts.

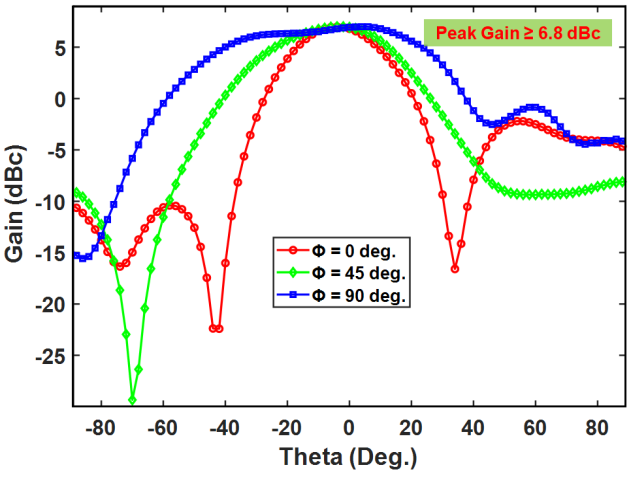

FIGURE 9. The measured gain levels for R_x mode at operational frequency of 2.45 GHz with $\Phi = 0°$, 45° and 90° cuts.

70 dB isolation levels over the entire matching bandwidth of 100 MHz as clearly reflected from measured results. As demonstrated earlier in simulation results, the path-loss isolation through spatial separation of each pair of T_x-R_x patches is around 27 dB and balanced feedings at both T_x and R_x ports elevate these isolation levels to 70 dB over the 100 MHz bandwidth. That means the balanced feeding contributes more than 43 dB isolation levels on the top of the spatial domain isolation.

As clear from Fig. 7(b), the simulated and measured S-parametrs closely follow each other except some significant deviations for the interport coupling results. These common deviations are based on the fact that the effects of connectorss and cables were not considered in simulations. Moreover, the fabrication accuracy and measurement tolerances also contribute to these deviations. However, the significant difference in simulated and measured interport coupling results is maninly due to additional magnitude and phase imbalances induced by cables used for interconnections of antenna elements and both baluns. Another factor which results in degradation of measured interport coupling levels is due to reflection from surrounding metallic objects in lab environment. Finally, the minor frequency shifting for measured S-parameter results is attributed the tolerances of the dielectric parameters like thickness and permittivity etc.

The far field characteristics of validation model of presented full duplex antenna system were endorsed through gain measurements at operational frequency of 2.45 GHz. These gain levels for both modes have been measured through two antenna method where the antenna under test had been used as a receiving antenna. The measured gain levels for $\Phi = 0°$, 45° and 90° far-field cuts are depicted in Fig. 8 and Fig. 9 for T_x and R_x modes respectively. The gain measurements performed for $\Phi = 0°$, 45° and 90° (azimuth plane) are intended to endorse the CP characteristics of the prototype. Due to unidirectional radiation characteristics of the presented antenna, the gain measurements for other

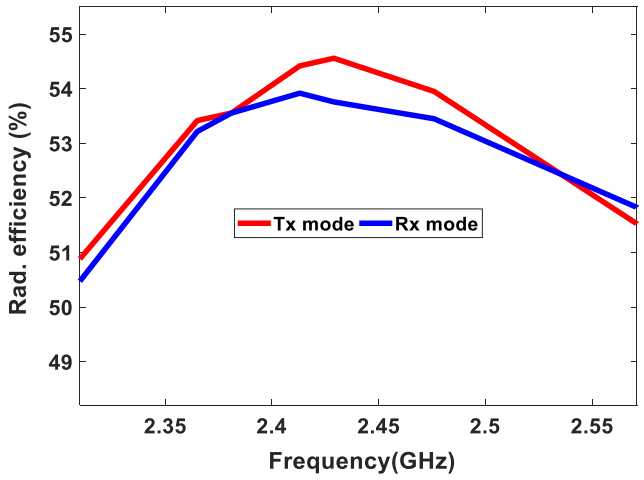

FIGURE 10. The recorded radiation efficiencies versus bandwidth (range of frequencies) results for T_x and R_x modes of prototype.

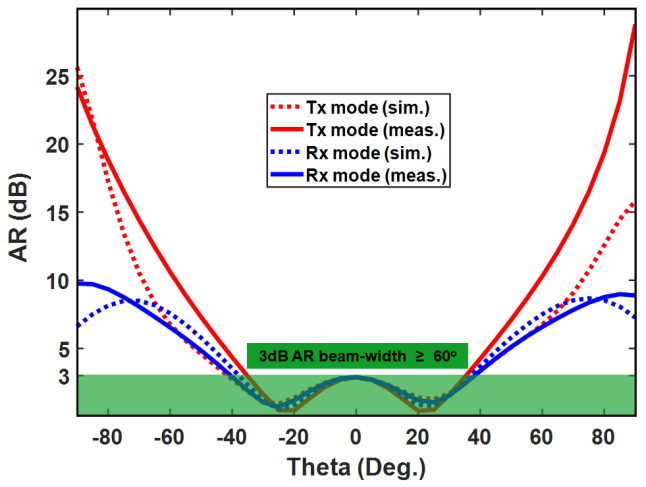

FIGURE 11. The experimental (measured) axial ratio (AR) versus elevation angle (θ) results at f = 2.45 GHz and $\Phi = 45°$ for T_x and R_x modes of co-CP full duplex antenna.

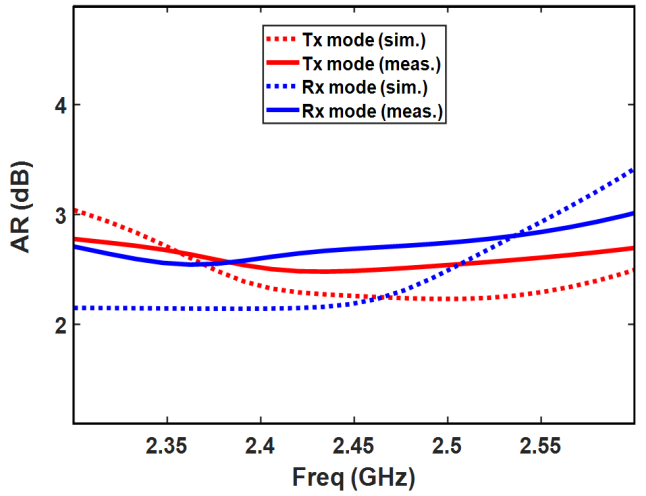

FIGURE 12. The measured axial ratio (AR) versus frequency results at $\theta = 0°$ and $\Phi = 45°$ for T_x and R_x modes of antenna prototype.

hemisphere ($\theta = 90°$ to $180°$) are not required. To record the gain levels for each port, the other port of the antenna system is terminated in 50 Ω matched load to avoid the reflections from that port. The measurement results depicted in Fig. 8 for T_x mode of antenna prototype offer better than 6.9 dBc peak gain at boresight ($\theta = 90°$) for $\Phi = 0°$, 45° and 90° cuts. Similarly, the recorded peak gains are also better than 6.8 dBc for $\Phi = 0°$, 45° and 90° cuts when the R_x port is used to record the power levels as clear from Fig. 9.

The balanced feeding approach offers better gain performance compared to single-ended excitation through reduced side lobes levels (SLL) i.e. reduced mutual coupling as reported in various earlier published works. The high loss FR-4 dielectric ($\tan\delta = 0.02$) can be replaced with low loss substrate to improve the radiation efficiencies and the resulting gains for both T_x and R_x modes. The resulting improvements in T_x and R_x gains can be validated through the simulations results for proposed antenna system by simply lowering the loss tangent values. For instance, 3 dB additional gain will be achieved if the radiation efficiency is doubled for antenna. It is important to note that both T_x and R_x modes have similar peak gain levels, same polarizations i.e. RHCP and overlapping -10 dB bandwidths along with high interport isolation levels as clear from measurements.

The radiation efficiency results for validation model (prototype) of presented antenna array were measured with the help of EMSCAN RFxpert near-field measurement setup. The measured radiation efficiencies are better than 53% for both T_x and R_x modes as clear from results presented in Fig. 10. The radiation efficiencies of the presented antenna can be improved through the use of low loss substrate for realization of prototype of this antenna.

The Fig. 11 depicts the simulated and measured axial ratio versus elevation angle (θ) results for presented antenna. The validation model of presented IBFD antenna characterizes 3dB axial ratio ($|AR| \leq 3dB$) beam-width of 60° for both T_x and R_x ports as clearly demonstrated through measured results in Fig. 11. Moreover, the recorded values of minimum AR are 2.6 dB and 2.8 dB for T_x and R_x modes respectively. These experimental characteristics for implemented antenna demonstrate nice CP characteristics over wider beam-width in elevation plane for both modes.

The simulated and measured AR versus frequency results for the presented antenna are given in Fig. 12. As obvious from these results, the validation model of presented IBFD antenna exhibits $|AR| \leq 3dB$ over the entire matching bandwidth of 100 MHz (2.40 GHz to 2.50 GHz). These AR versus frequency measurements endorse the intended CP characteristics over the entire matching bandwidth of antenna for both T_x and R_x ports.

IV. NOVELTY AND CONTRIBUTIONS OF PRESENTED ANTENNA SYSTEM

The performance comparison of the presented antenna system with some of the previously reported co-CP antennas

TABLE 1. The performance comparison of presented antenna with some of the previously reported co-polarized antennas.

Ref.	-10dB Bandwidth	Avg. Isolation/ Bandwidth	Tx/Rx Polarization	SIC Topology
[20]	2 GHz for VSWR < 2.2	50 dB/ 2 GHz	RHCP (T_x/R_x)	Near field cancellation
[21]	0.56 GHz - 2.75 GHz	27 dB/ 2.2 GHz	RHCP (T_x/R_x)	Near field cancellation
[39]	1.2 GHz	40 dB/1.2 GHz	RHCP (T_x/R_x)	Near field cancellation
[40]	75 MHz	47 dB/ 75 MHz	LHCP (T_x/R_x)	Near field cancellation
[41]	100 MHz	47 dB/100 MHz	RHCP/LHCP	Near field cancellation
[42]	520 MHz	37 dB/ 520 MHz	Linear pol. (T_x/R_x)	Near field cancellation
[43]	100 MHz	41 dB/100 MHz	RHCP (T_x/R_x)	Near field cancellation
[44]	100 MHz	41 dB/100 MHz	RHCP (T_x/R_x)	Near field cancellation
This Design	**≥ 100 MHz**	**70 dB/ 100 MHz**	**RHCP (T_x/R_x)**	**Near field cancellation**

is detailed in table 1. The selected antennas for comparison purpose also utilize near filed SIC to improve interport isolation levels. The validation model (prototype) for our presented co-RHCP antenna in this work features very high levels of port to port isolation levels compared to previously reported co-CP antennas intended for full duplex applications. These elevated interport isolation levels are ascribed to effective suppression of resulting SI and complex inter-element coupling through well-balanced feeding networks employed at both T_x and R_x ports of presented antenna with same polarization for both modes.

Compared to earlier reported co-CP antennas, the novelty of antenna system presented in this work is high interport isolation across the entire -10 dB impedance bandwidth of antenna along with same gain levels for both T_x and R_x modes. These high isolation levels along with RHCP polarization characteristics for both T_x and R_x modes offer the real gains of full duplex wireless operation without polarization-duplexing for bidirectional links. Moreover, the CP based wireless links avoid the inherent polarization mismatch losses in wireless links with linearly polarized characteristics. Furthermore, the presented antenna array offers better gain performance compared to single-element based IBFD antennas which will improve the coverage or range of wireless communication for given T_x power.

V. CONCLUSION

A co-RHCP printed antenna with unidirectional radiation patterns is presented which achieves very high interport isolation over entire impedance of antenna for S-band full duplex applications. The superior in-band amplitude and out-of-phase balance performance of feeding networks features excellent passive SIC operation for presented antenna array with co-circularly polarized characteristics. The employed balanced feedings also result in reduced mutual coupling between patches to achieve better gain levels through effective lower side lobe levels (SLL). The performance of the presented antenna prototype has been endorsed through measured impedance bandwidths for both T_x and R_x ports, port to port coupling levels, axial ratio versus frequency, axial ratio versus elevation angle parameters, and resulting antenna gains for both modes. As the insertion loss of the employed balun is very low (≤0.5 dB) across the intended bandwidth so the antenna gain performance will not be degraded when the baluns are used for balanced excitations of both modes. The gain of the presented antenna can be enhanced through implementation of given structure on low loss substrate which will offer improved radiation efficiency.

REFERENCES

[1] S. Wu, H. Guo, J. Xu, S. Zhu, and H. Wang, "In-band full duplex wireless communications and networking for IoT devices: Progress, challenges and opportunities," *Future Gener. Comput. Syst.*, vol. 92, pp. 705–714, Mar. 2019.

[2] J. Wang, A. Jin, D. Shi, L. Wang, and H. Shen, "Spectral efficiency improvement with 5G technologies: Results from field tests," *IEEE J. Sel. Areas Commun.*, vol. 35, no. 8, pp. 1867–1875, Aug. 2017.

[3] M. Heino, S. N. Venkatasubramanian, C. Icheln, and K. Haneda, "Design of wavetraps for isolation improvement in compact in-band full-duplex relay antennas," *IEEE Trans. Antennas Propag.*, vol. 64, no. 3, pp. 1061–1070, Mar. 2016.

[4] J. Marašević, J. Zhou, H. Krishnaswamy, Y. Zhong, and G. Zussman, "Resource allocation and rate gains in practical full-duplex systems," *IEEE/ACM Trans. Netw.*, vol. 25, no. 1, pp. 292–305, Feb. 2017.

[5] R. Li, A. Masmoudi, and T. Le-Ngoc, "Self-interference cancellation with nonlinearity and phase-noise suppression in full-duplex systems," *IEEE Trans. Veh. Technol.*, vol. 67, no. 3, pp. 2118–2129, Mar. 2018.

[6] C.-X. Mao, S. Gao, and Y. Wang, "Dual-band full-duplex Tx/Rx antennas for vehicular communications," *IEEE Trans. Veh. Technol.*, vol. 67, no. 5, pp. 4059–4070, May 2018.

[7] K. E. Kolodziej, B. T. Perry, and J. S. Herd, "In-band full-duplex technology: Techniques and systems survey," *IEEE Trans. Microw. Theory Techn.*, vol. 67, no. 7, pp. 3025–3041, Jul. 2019.

[8] C. D. Nwankwo, L. Zhang, A. Quddus, M. A. Imran, and R. Tafazolli, "A survey of self-interference management techniques for single frequency full duplex systems," *IEEE Access*, vol. 6, pp. 30242–30268, 2018.

[9] H. Nawaz and I. Tekin, "Compact dual-polarised microstrip patch antenna with high interport isolation for 2.5 GHz in-band full-duplex wireless applications," *IET Microw., Antennas Propag.*, vol. 11, no. 7, pp. 976–981, 2017.

[10] M. Heino, D. Korpi, T. Huusari, E. Antonio-Rodriguez, and S. Venkatasubramanian, "Recent advances in antenna design and interference cancellation algorithms for in-band full duplex relays," *IEEE Commun. Mag.*, vol. 53, no. 5, pp. 91–101, May 2015.

[11] M. S. Amjad, H. Nawaz, K. Özsoy, Ö. Gürbüz, and I. Tekin, "A low-complexity full-duplex radio implementation with a single antenna," *IEEE Trans. Veh. Technol.*, vol. 67, no. 3, pp. 2206–2218, Mar. 2018.

[12] D. Korpi, T. Riihonen, V. Syrjälä, L. Anttila, M. Valkama, and R. Wichman, "Full-duplex transceiver system calculations: Analysis of ADC and linearity challenges," *IEEE Trans. Wireless Commun.*, vol. 13, no. 7, pp. 3821–3836, Jul. 2014.

[13] D. El Hadri, A. Zakriti, A. Zugari, M. El Ouahabi, and J. El Aoufi, "High isolation and ideal correlation using spatial diversity in a compact MIMO antenna for fifth-generation applications," *Int. J. Antennas Propag.*, vol. 2020, Jul. 2020, Art. no. 2740920.

[14] D. S. Chandu and S. S. Karthikeyan, "A novel broadband dual circularly polarized microstrip-fed monopole antenna," *IEEE Trans. Antennas Propag.*, vol. 65, no. 3, pp. 1410–1415, Mar. 2017.

[15] Y. Shen, S.-G. Zhou, G.-L. Huang, and T.-H. Chio, "A compact dual circularly polarized microstrip patch array with interlaced sequentially rotated feed," *IEEE Trans. Antennas Propag.*, vol. 64, no. 11, pp. 4933–4936, Nov. 2016.

[16] J. Wu, Y. J. Cheng, and Y. Fan, "Wide-band dual-polarized planar array antenna for K/Ka-band wireless communication," *Micro. Opt. Technol. Lett.*, vol. 58, no. 10, pp. 2377–2381, Oct. 2016.

[17] J. Wu, Y. J. Cheng, H. B. Wang, Y. C. Zhong, D. Ma, and Y. Fan, "A wideband dual circularly polarized full-corporate waveguide array antenna fed by triple-resonant cavities," *IEEE Trans. Antennas Propag.*, vol. 65, no. 4, pp. 2135–2139, Apr. 2017.

[18] S. G. Zhou, G. L. Huang, T. H. Chio, J. J. Yang, and G. Wei, "Design of a wideband dual-polarization full-corporate waveguide feed antenna array," *IEEE Trans. Antennas Propag.*, vol. 63, no. 11, pp. 4775–4782, Nov. 2015.

[19] M. Yilan, H. Ayar, H. Nawaz, O. Gurbuz, and I. Tekin, "Monostatic antenna in-band full duplex radio: Performance limits and characterization," *IEEE Trans. Veh. Technol.*, vol. 68, no. 5, pp. 4786–4799, May 2019.

[20] E. A. Etellisi, M. A. Elmansouri, and D. S. Filipovic, "Wideband monostatic simultaneous transmit and receive (STAR) antenna," *IEEE Trans. Antennas Propag.*, vol. 64, no. 1, pp. 6–15, Jan. 2016.

[21] M. A. Elmansouri, A. J. Kee, and D. S. Filipović, "Wideband antenna array for simultaneous transmit and receive (STAR) applications," *IEEE Antennas Wireless Propag. Lett.*, vol. 16, pp. 1277–1280, 2017.

[22] E. Yetisir, C.-C. Chen, and J. L. Volakis, "Wideband low profile multiport antenna with omnidirectional pattern and high isolation," *IEEE Trans. Antennas Propag.*, vol. 64, no. 9, pp. 3777–3786, Sep. 2016.

[23] E. A. Etellisi, M. A. Elmansouri, and D. S. Filipović, "Wideband multimode monostatic spiral antenna STAR subsystem," *IEEE Trans. Antennas Propag.*, vol. 65, no. 4, pp. 1845–1854, Apr. 2017.

[24] Q. Li and T.-Y. Shih, "Characteristic-mode-based design of planar in-band full-duplex antennas," *IEEE Open J. Antennas Propag.*, vol. 1, pp. 329–338, 2020.

[25] X. Wang, W. Che, W. Yang, W. Feng, and L. Gu, "Self-interference cancellation antenna using auxiliary port reflection for full-duplex application," *IEEE Antennas Wireless Compon. Lett.*, vol. 16, pp. 2873–2876, 2017.

[26] A.-N. Nguyen, V. Hoang Le, N. Nguyen-Trong, M. Radfar, A. Ebrahimi, K. Phan, and A. Desai, "Dual-polarized slot antenna for full-duplex systems with high isolation," *IEEE Trans. Antennas Propag.*, vol. 69, no. 11, pp. 7119–7124, Nov. 2021.

[27] H. Nawaz, Ö. Gürbüz, and I. Tekin, "High isolation slot coupled antenna with integrated tunable self-interference cancellation circuitry," *Electron. Lett.*, vol. 54, no. 23, pp. 1311–1312, Nov. 2018.

[28] S. Khaledian, F. Farzami, B. Smida, and D. Erricolo, "Inherent self-interference cancellation for in-band full-duplex single-antenna systems," *IEEE Trans. Microw. Theory Techn.*, vol. 66, no. 6, pp. 2842–2850, Jun. 2018.

[29] M. Yang, S.-W. Jeon, and D. K. Kim, "Interference management for in-band full-duplex vehicular access networks," *IEEE Trans. Veh. Technol.*, vol. 67, no. 2, pp. 1820–1824, Feb. 2018.

[30] T. Riihonen, D. Korpi, O. Rantula, H. Rantanen, T. Saarelainen, and M. Valkama, "Inband full-duplex radio transceivers: A paradigm shift in tactical communications and electronic warfare?" *IEEE Commun. Mag.*, vol. 55, no. 10, pp. 30–36, Oct. 2017.

[31] H. Chou, Y. Kao, C. Peng, Y. Wang, and T. Chu, "An X-band frequency-modulated continuous-wave radar sensor system with a single-antenna interface for ranging applications," *IEEE Trans. Microw. Theory Techn.*, vol. 66, no. 9, pp. 4216–4231, Sep. 2018.

[32] N. Reiskarimian, T. Dinc, J. Zhou, T. Chen, M. B. Dastjerdi, J. Diakonikolas, G. Zussman, and H. Krishnaswamy, "One-way ramp to a two-way highway: Integrated magnetic-free nonreciprocal antenna interfaces for full-duplex wireless," *IEEE Microw. Mag.*, vol. 20, no. 2, pp. 56–75, Feb. 2019.

[33] H. Nawaz and I. Tekin, "Double-differential-fed, dual-polarized patch antenna with 90 dB interport RF isolation for a 2.4 GHz in-band full-duplex transceiver," *IEEE Antennas Wireless Propag. Lett.*, vol. 17, no. 2, pp. 287–290, Feb. 2018.

[34] G. Chaudhary, J. Jeong, and Y. Jeong, "Differential fed antenna with high self-interference cancellation for in-band full-duplex communication system," *IEEE Access*, vol. 7, pp. 45340–45348, 2019.

[35] H. Nawaz and I. Tekin, "Dual-polarized, differential fed microstrip patch antennas with very high interport isolation for full-duplex communication," *IEEE Trans. Antennas Propag.*, vol. 65, no. 12, pp. 7355–7360, Dec. 2017.

[36] S. Khaledian, F. Farzami, B. Smida, and D. Erricolo, "Robust self-interference cancellation for microstrip antennas by means of phase reconfigurable coupler," *IEEE Trans. Antennas Propag.*, vol. 66, no. 10, pp. 5574–5579, Oct. 2018.

[37] H. Nawaz, A. U. Niazi, M. A. Basit, F. Shaukat, and M. Usman, "Dual-polarized, monostatic antenna array with improved T_x–R_x isolation for 2.4 GHz in-band full duplex applications," *Int. J. Microw. Wireless Technol.*, vol. 12, no. 5, pp. 398–408, 2020.

[38] S. Lin, J. Wang, Y. Deng, and G. Zhang, "A new compact ultra-wideband balun for printed balanced antennas," *J. Electromagn. Waves Appl.*, vol. 29, no. 12, pp. 1570–1579, Aug. 2015.

[39] J. Wu, M. Li, and N. Behdad, "A wideband, unidirectional circularly polarized antenna for full-duplex applications," *IEEE Trans. Antennas Propag.*, vol. 66, no. 3, pp. 1559–1563, Mar. 2018.

[40] H. Nawaz, A. U. Niazi, M. Abdul Basit, and M. Usman, "Single layer, differentially driven, LHCP antenna with improved isolation for full duplex wireless applications," *IEEE Access*, vol. 7, pp. 169796–169806, 2019.

[41] J. Ha, M. A. Elmansouri, P. V. Prasannakumar, and D. S. Filipović, "Monostatic co-polarized full-duplex antenna with left- or right-hand circular polarization," *IEEE Trans. Antennas Propag.*, vol. 65, no. 10, pp. 5103–5111, Oct. 2017.

[42] L. Sun, Y. Li, Z. Zhang, and Z. Feng, "Compact co-horizontally polarized full-duplex antenna with omnidirectional patterns," *IEEE Antennas Wireless Propag. Lett.*, vol. 18, no. 6, pp. 1154–1158, Jun. 2019.

[43] D. Wu, Y.-X. Sun, B. Wang, and R. Lian, "A compact, monostatic, co-circularly polarized simultaneous transmit and receive (STAR) antenna with high isolation," *IEEE Antennas Wireless Propag. Lett.*, vol. 19, no. 7, pp. 1127–1131, Jul. 2020.

[44] Z. Zhou, Y. Li, J. Hu, Y. He, Z. Zhang, and P.-Y. Chen, "Monostatic copolarized simultaneous transmit and receive (STAR) antenna by integrated single-layer design," *IEEE Antennas Wireless Propag. Lett.*, vol. 18, no. 3, pp. 472–476, Mar. 2019.

HAQ NAWAZ received the B.Sc. degree in electrical engineering and the master's degree in telecommunication engineering from the University of Engineering and Technology (UET), Taxila, Pakistan, in 2005 and 2012, respectively, and the Ph.D. degree in electronic engineering from Sabanci University, Istanbul, Turkey.

From January 2017 to June 2018, he worked as a Postdoctoral Research Fellow with the Faculty of Engineering and Natural Sciences (FENS), Sabanci University. From 2006 to 2009, he was a RF Design Engineer with the Space and Upper Atmosphere Research Commission (SUPARCO), Pakistan. From November 2009 to April 2021, he worked as a Faculty Member in electrical and electronics engineering with the UET. He is currently working as an Associate Professor at the Department of Electrical Engineering, University of Engineering and Technology (UET), Lahore, Pakistan. He has authored more than 30 research articles published in renowned international journals in addition to one patent in U.S. patent and trademark office's and several papers in IEEE conferences. His research interests include full duplex antenna design, RF circuits design and measurements for radar and satellite systems, beam-switched and phased scanning array antennas design, and indoor positioning systems design. He is a part of editorial teams of several journals, including the IEEE Transactions on Antennas and Propagation, the IEEE Transactions on Vehicular Technology, the IEEE Transactions on Microwave Theory and Techniques, the IEEE Wireless Communications, the IEEE Transactions on Aerospace and Electronic Systems, the IEEE Transactions on Industrial Electronics, and IEEE Access.

AHMAD UMAR NIAZI received the B.Sc. degree in electrical engineering with specialization in communication and electronics from the University of Engineering and Technology (UET), Lahore, Pakistan, in 2001, and the master's degree in electrical engineering from the University of Engineering and Technology (UET), Taxila, Pakistan, in 2012, where he is currently pursuing the Ph.D. degree in electrical engineering.

He served at local private and public sector industry/organizations from 2001 to 2006. He joined the UET Taxila, Sub Campus Chakwal, Pakistan. From 2007 to 2012, he worked as a Lecturer in electronics engineering. Since 2012, he has been working as an Assistant Professor at the Department of Electronics Engineering, UET Taxila. His research interests include microwave antenna design, antennas for 5G applications, full duplex antenna design, RF circuits design, beam-switched and phased scanning array antennas, and multi-band jamming techniques.

AHSEN TAHIR received the M.S. degree in computer engineering from the University of Michigan, Ann Arbor, MI, USA, and the Ph.D. degree from Glasgow Caledonian University, Glasgow, U.K. He is currently working as an Assistant Professor at the Department of Electrical Engineering, University of Engineering and Technology, Lahore, Pakistan. He is also an experienced researcher. He has research/teaching experience with prestigious institutes, including Glasgow Caledonian University (U.K.), and Edinburgh Napier University (U.K). He also develops re-configurable embedded hardware accelerators for machine and deep learning applications. He also develops mathematical models for various research problems and has experience with radio frequency sensing, antennas and applications. His research interests include machine learning/deep learning for healthcare applications.

NOMAN AHMAD received the B.Sc. degree in electronics engineering from the University of Engineering and Technology (UET), Taxila, Sub Campus Chakwal, Pakistan, in 2019. He is currently pursuing the master's degree in electrical engineering (RF and microwave) with the Research Institute for Microwave and Millimeter-Wave Studies (RIMMS), National University of Sciences and Technology (NUST), Islamabad, Pakistan. His research interests include passive beam-forming-networks (BFNs), phased array scanning antennas, in-band-full-duplex (IBFD) communications, and frequency-modulated-continuous-wave (FMCW) radars.

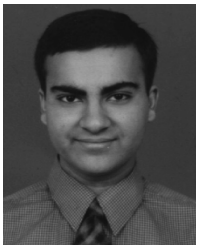

USMAN MASUD received the B.Sc. degree in electrical engineering from the University of Engineering and Technology, Taxila, in 2005, the M.S. degree in electrical engineering in Germany, in 2010, and the Ph.D. degree (by research work), in 2014. He has been involved in multiple research areas at the moment and finds deep interest in laser-based biomedical applications. His research interests include laser systems, biomedical sensors, spectroscopic applications, and wireless networks. He has been an Active Member of Verband der Elektrotechnik, Elektronik und Informationstechnik e.V. (VDE) for several years.

TURKE ALTHOBAITI received the B.Sc. degree in computer science from Taif University, Saudi Arabia, in 2009, the M.Sc. degree in computer science from Ball State University, USA, in 2014, and the Ph.D. degree in computer science from the University of the West of Scotland, U.K., in 2019. He is currently an Assistant Professor with Northern Border University, Saudi Arabia. His research interests include affective computing and machine learning.

ABDULLAH ALHUMAIDI ALOTAIBI is currently affiliated with the Department of Science and Technology, College of Ranyah, Taif University, Taif, Saudi Arabia. He is also the Head of the Innovation and Entrepreneurship Center, Taif University. He worked in the areas of Doppler radar, OFDM modulation, biomedical communication, and body sensor networks. His research interests include deep learning (artificial intelligence), feature extraction, health care, image classification, medical image processing, patient monitoring, hyperspectral imaging, image motion analysis, image representation, indoor radio, and learning.

NAEEM RAMZAN (Senior Member, IEEE) received the M.Sc. degree in telecommunications from the University of Brest, France, in 2004, and the Ph.D. degree in electronics engineering from the Queen Mary University of London, London, U.K., in 2008. He is currently a Full Professor of artificial intelligence and the Director of the Affective and Human Computing for Smart Environment (AHCSE) Research Centre, University of the West of Scotland (UWS), U.K. He has authored or coauthored more than 200 research publications, including journals, book chapters, and standardization contributions. His research interests include cross-disciplinary and industry focused and include AI/machine learning, affective computing and multimedia processing, analysis and communication, video quality evaluation, brain-inspired multimodal cognitive technology, big data analytics, affective computing, the IoT/smart environments, natural multi-modal human–computer interaction, and eHealth/connected Health.